Appl Petrochem Res (2015) 5:305–311
DOI 10.1007/s13203-015-0119-9

ORIGINAL ARTICLE

Vacuum ultraviolet photofragmentation of octadecane: photoionization mass spectrometric and theoretical investigation

Jing Xu[1] · Pengpeng Sang[1] · Lianming Zhao[1] · Wenyue Guo[1] · Fei Qi[2] · Wei Xing[1] · Zifeng Yan[3]

Received: 17 May 2015 / Accepted: 21 June 2015 / Published online: 7 July 2015

Abstract The photoionization and fragmentation of octadecane were investigated with infrared laser desorption/tunable synchrotron vacuum ultraviolet (VUV) photoionization mass spectrometry (IRLD/VUV PIMS) and theoretical calculations. Mass spectra of octadecane were measured at various photon energies. The fragment ions were gradually detected with the increase of photon energy. The main fragment ions were assigned to radical ions ($C_nH_{2n+1}^+$, $n = 4$–11) and alkene ions ($C_nH_{2n}^+$, $n = 5$–10). The ionization energy of the precursor and appearance energy of ionic fragments were obtained by measuring the photoionization efficiency spectrum. Possible formation pathways of the fragment ions were discussed with the help of density functional theory calculations.

Keywords Synchrotron vacuum ultraviolet · Photoionization · Alkanes · Mass spectrometry

✉ Lianming Zhao
lmzhao@upc.edu.cn

✉ Zifeng Yan
zfyancat@upc.edu.cn

[1] College of Science, China University of Petroleum, Qingdao 266580, Shandong, People's Republic of China

[2] National Synchrotron Radiation Laboratory, University of Science and Technology of China, Hefei 230029, Anhui, People's Republic of China

[3] State Key Laboratory of Heavy Oil Processing, Key Laboratory of Catalysis, China University of Petroleum, Qingdao 266580, People's Republic of China

Introduction

With the increasing demand for energy and ongoing depletion of light oil resources, high-efficient use of heavy oils is becoming more and more attractive. To explore the extreme refinement of heavy oils, it is necessary to deeply understand their compositions and structures [1, 2]. It is known that petroleum residues can be divided into saturates, aromatics, resins, and asphaltenes (SARA) according to the molecular polarity and solubility. In general, saturates are primarily consist of saturated alkanes and cycloalkanes. On the other hand, the pyrolysis of crude oil is considered as one of major sources of natural gas. In crude oil, one of the main components is alkanes. Therefore, study of alkane cracking is important to understand the genesis of natural gas. As is well known, octadecane is a prototype of the class of *n*-alkanes, and thus it is very interesting to study its property and decomposition mechanism.

In recent decades, various techniques have been applied to analyze petroleum [3–9]. These methods include fluorescent indicator adsorption [4], infrared (IR)/Fourier-transform infrared (FTIR) spectroscopy [7], nuclear magnetic resonance (NMR) spectroscopy [8], mass spectrometry (MS) [3, 6], gas chromatography (GC) [9], and so on. Among them, MS always shows the predominance in the analysis of petroleum due to its accuracy and high speed. Recently, as a powerful detection tool, photoionization mass spectrometry (PIMS) has been used extensively for analyzing organic analytes and studying combustion [10–12]. However, experimental measurements of photoionization for alkanes are scarce. Kameta et al. measured the photoionization and dissociation properties of methane, ethane, propane, cyclopropane, and *n*-butane using a double ionization chamber combined with synchrotron

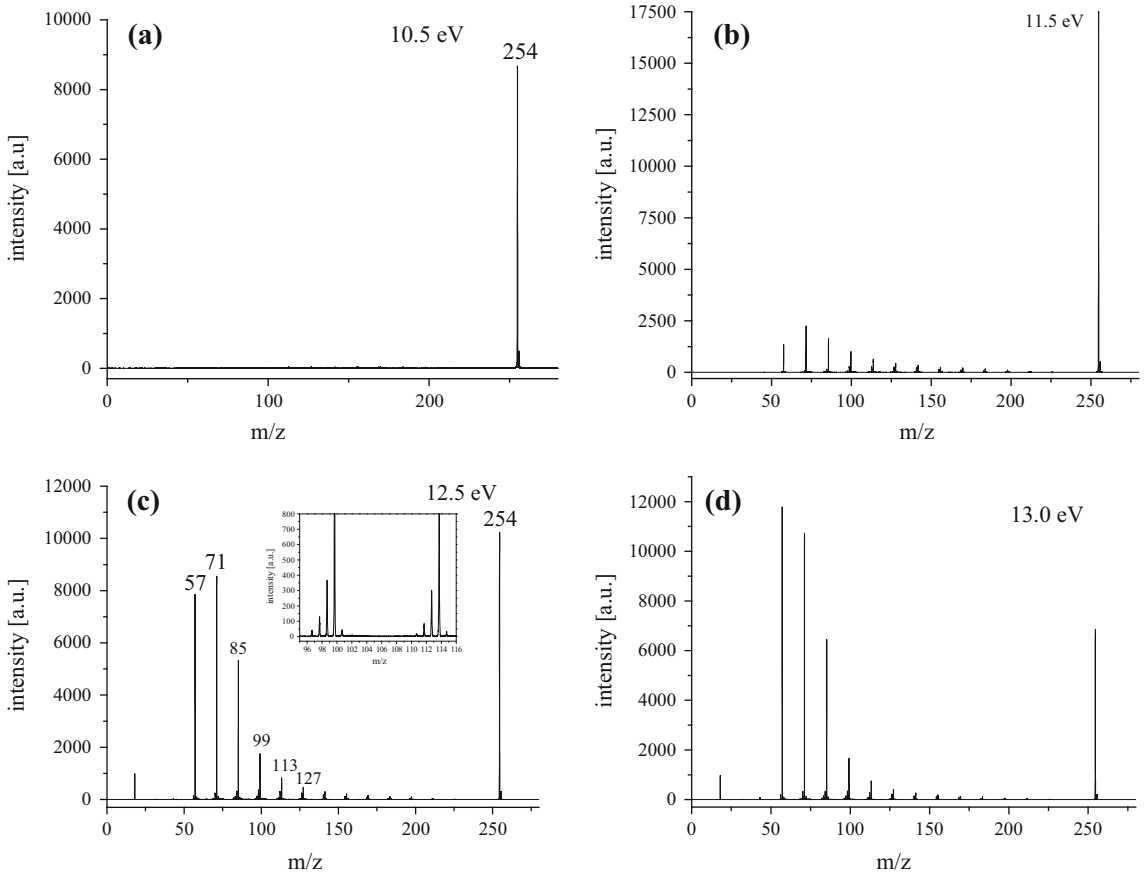

Fig. 1 Photoionization mass spectra of octadecane at photon energies of **a** 10.5 eV, **b** 11.5 eV, **c** 12.5 eV, and **d** 13.0 eV

radiation [13]. Steiner et al. reported the photoionization and subsequent dissociation of all saturated paraffins from C_2 to C_6, plus *n*-heptane and *n*-octane using a mass spectrometer combined with a Seya–Namioka monochromator [14]. Schoen measured the ionization and ion-fragmentation cross sections of ethane, propane, *n*-butane, *n*-pentane, cyclopropane, etc., under vacuum ultraviolet radiation [15]. The photoionization cross sections of *n*-pentane, *n*-hexane, *n*-heptane, *n*-octane, *n*-nonane, and *n*-decane were measured exclusively at 10.5 eV by Adam and Zimmermann [16]. The near-threshold photoionization cross sections for methane, ethane, propane, *n*-butane, cyclopropane, and methylcyclopentane were measured by Cool and coworkers [17] using PIMS combined with vacuum ultraviolet (VUV) synchrotron radiation. Recently, the photoionization and dissociative photoionization cross sections of eleven *n*-alkanes, three cyclo-alkanes, and iso-octane were measured by Zhou et al., utilizing tunable synchrotron VUV photoionization and molecular-beam mass spectrometry [18]. Although photoionization properties are available for some small alkanes, the photoionization investigations of large alkanes are very sparse.

In this work, we investigated the photoionization and fragmentation behavior of octadecane using infrared laser desorption/tunable VUV PIMS (IRLD/VUV PIMS) and theoretical calculations. The photoionization mass spectra of octadecane were obtained at different photon energies.

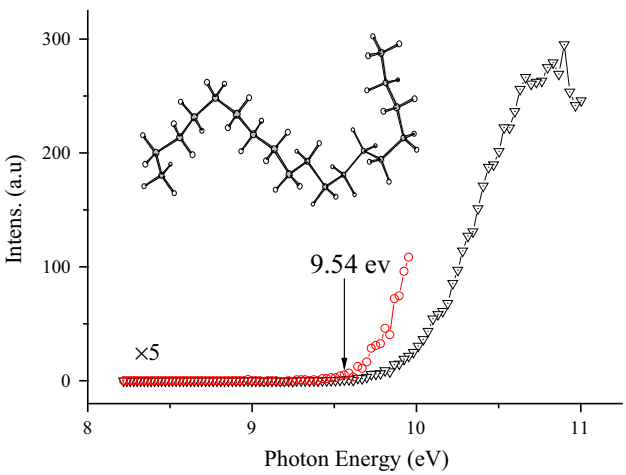

Fig. 2 PIE spectrum of molecular ion

The ionization energy (IE) of octadecane and appearance energy (AE) of fragments were obtained by measuring the photoionization efficiency (PIE) spectrum. Furthermore, the major dissociation pathways to form radical $C_nH_{2n+1}^+$ ($n = 4$–11) and alkene $C_nH_{2n}^+$ ($n = 5$–10) fragments were presented on the basis of density functional theory calculations.

Experimental and theoretical methods

Experimental method

The experiment was completed at the National Synchrotron Radiation Laboratory, Hefei, China. The IR LD/VUV PIMS setup was described in detail in previous publications [19, 20]. Briefly, the instrument used a Nd:YAG laser beam (Surelite I-20; Continuum, Santa Clara, CA, USA; wavelength 1064 nm, repetition rate 10 Hz) for desorption of samples mounted on a stainless steel substrate. To generate the plume of intact neutral molecules, the laser power for desorption was controlled at about 6 mJ/pulse. The desorbed neutral molecules in the gas phase were ionized by the crossed synchrotron VUV light, and the generated ions were detected by a home-made reflection time-of-flight (RTOF) mass spectrometer. The ion signals were amplified by a preamplifier (VT120C, EG & G, ORTEC, U.S.A.) and recorded by a P7888 multiscaler (FAST Comtec, Germany). Time delay between the laser and the pulse of

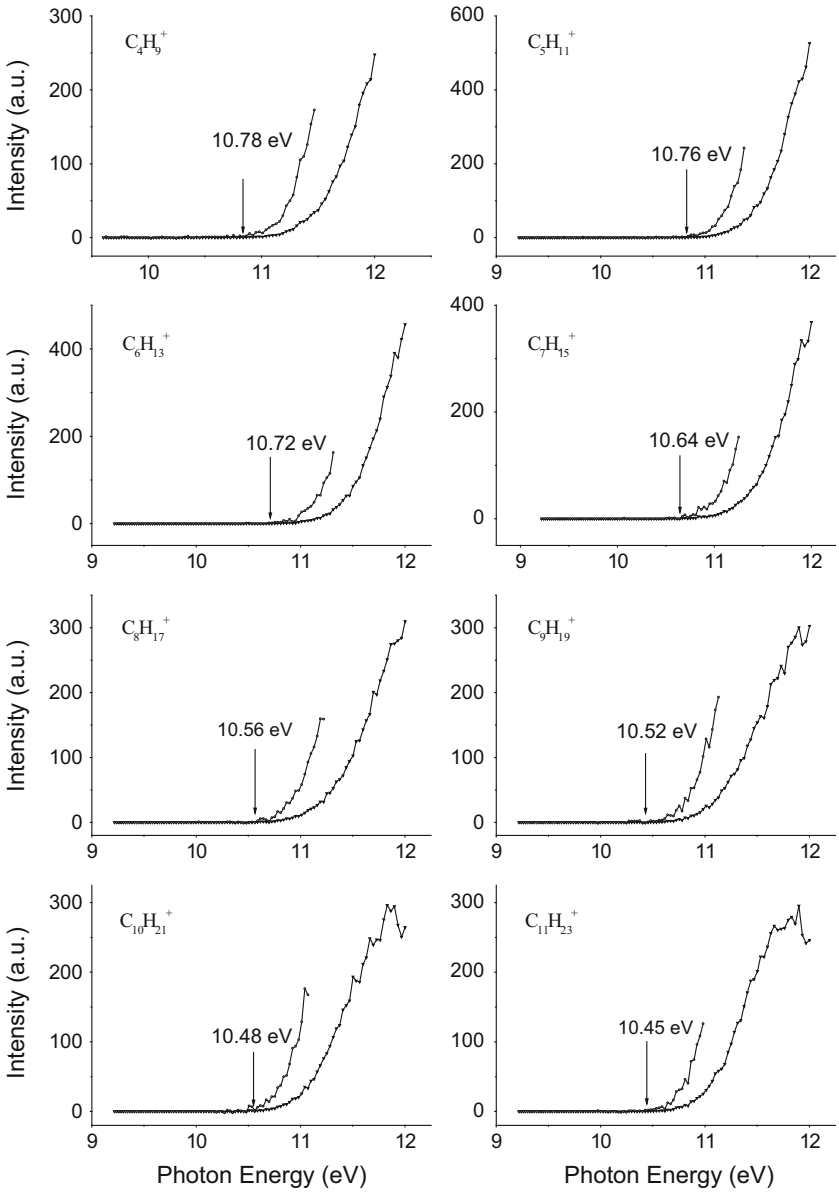

Fig. 3 PIE spectra of $C_nH_{2n+1}^+$ radical ions

repeller field of RTOF is 150 μs, which was controlled by a homemade pulse/delay generator.

Synchrotron VUV radiation from an undulator beamline of 800 MeV electron storage ring of the NSRL was monochromatized by a 1 m Seya–Namioka monochromator with a laminar grating (1500 grooves mm^{-1}, Horiba Jobin–Yvon, France). The grating covered the photon energy range from 7.8 to 24 eV with the energy resolution ($E/\Delta E$) of about 1000. The monochromator was calibrated with known IEs of inert gases. A gas filter filled with neon or argon was used to eliminate higher order harmonic radiation. The average photon flux was measured to be 1×10^{13} photons/s. A silicon photodiode (SXUV-100, International Radiation Detectors Inc., U.S.A.) was used to monitor the photon flux for normalizing ion signals.

Computational method

All the theoretical calculations were performed using Gaussian 03 program package [21]. The geometries were full optimized using the hybrid B3LYP functional in conjunction with the 6-31+G(d,p) basis set [22]. The harmonic frequencies were calculated at the same level to identify the minima and transation state (TS). The zero-point energies (ZPE) corrections were also obtained from the frequency calculations. Furthermore, the photoionization and dissociation were studied at the B3P86/6-31++G (d, p) level. All the theoretical energies used in this work are electronic energies with ZPE correction. The AE of ionic fragment is defined as $E_{AE} = E_{max} - E_0$, in which E_{max} refers to the highest energy barrier involved in the formation pathway of corresponding ionic fragment and E_0 is the absolute energy of neutral molecular [23]. Natural bond orbital (NBO) analysis was carried out to characterize the bonds and interactions inside some important species [24].

Results and discussion

Photoionization mass spectra

Figure 1 shows the photoionization mass spectra of octadecane at different photon energies. At low photon energy (10.5 eV), the molecular ion at m/z 254 was detected by near-threshold single-photon ionization (SPI). The fragment ions are negligible, accounting for a soft ionization technique [25–27]. When the photon energy increases to 11.5 eV, fragment ions are formed gradually. At the photon energies of 12.5 and 13 eV, the intensity of relevant fragment ions increases substantially. As shown in Fig. 1, groups of hydrocarbons in fragment ions are clearly observed, and each group has about 2–3 strong ion peaks. The mass difference between two adjacent groups is 14 m/z units, namely, CH_2 group, while two adjacent ion peaks in each group have a mass difference of 1 m/z. These peaks can be mainly attributed to two classes of hydrocarbons: radical hydrocarbon ions ($C_nH^+_{2n+1}$) and alkene ions ($C_nH^+_{2n}$). For example, at the photon energy of 12.5 eV, the main fragment ions are radical ions $C_nH^+_{2n+1}$ ($n = 4$–11) and alkene ions $C_nH^+_{2n}$ ($n = 5$–10). The intensity of peaks follows the order of m/z 71 > 57 > 85 > 99 > 113. Correspondingly, the fragment ions could be assigned to $C_5H_{11}^+$, $C_4H_9^+$, $C_6H_{13}^+$, $C_7H_{15}^+$, and $C_8H_{17}^+$, respectively. At the left of each radical ion, there is a weak distribution of $C_nH^+_{2n}$ and $C_nH^+_{2n-1}$ ions. Similar results have been reported in the electron-impact (EI) mass spectrum of octadecane at 70 eV [28].

Photoionization efficiency spectra

The IE value can be measured by scanning PIE spectra, which are obtained by consecutively altering VUV photon energy. The neutral plume of octadecane was generated in the IR laser desorption process. Thus, the hot-band effect will result in a thermal tail in PIE of the molecular ion, which may make it difficult to accurately determine the onset threshold. In addition, weak Franck–Condon factor near the ionization threshold causes a not-obvious onset. Some methods have been employed to determine the ionization threshold [29–31]. In this work, it is assumed that

Table 1 The calculated and experimental energies of products and relevant transition states with respect to neutral octadecane (in eV)

Formula	Calcd	Expt (AE)
$C_4H_9^+ + C_{14}H_{29}$	11.02	10.78
$C_5H_{11}^+ + C_{13}H_{27}$	10.84	10.76
$C_6H_{13}^+ + C_{12}H_{25}$	10.81	10.72
$C_7H_{15}^+ + C_{11}H_{23}$	10.80	10.64
$C_8H_{17}^+ + C_{10}H_{21}$	10.78	10.56
$C_9H_{19}^+ + C_9H_{19}$	10.77	10.52
$C_{10}H_{21}^+ + C_8H_{17}$	10.68	10.48
$C_{11}H_{23}^+ + C_7H_{15}$	10.66	10.45
$C_5H_{10}^+ + C_{13}H_{28}$	10.28	–
$C_6H_{12}^+ + C_{12}H_{26}$	10.23	–
$C_7H_{14}^+ + C_{11}H_{24}$	10.20	–
$C_8H_{16}^+ + C_{10}H_{22}$	10.18	–
$C_9H_{18}^+ + C_9H_{20}$	10.17	–
$C_{10}H_{20}^+ + C_8H_{18}$	10.17	–
TS1	10.82	10.56
TS2	10.75	10.52
TS3	10.70	10.48
TS4	10.68	10.45
TS5	10.64	10.43
TS6	10.58	10.42

the thermal tail near ionization threshold is dominantly affected by thermal energy from laser heating. The PIE spectrum of octadecane is shown in Fig. 2. It can be found that the IE of octadecane is 9.54 ± 0.05 eV based on the first discernible onset. The calculated adiabatic IE value of octadecane is 9.46 eV by the B3P86/6-31++G(d,p)// B3LYP/6-31+G(d,p) method, according well with the experimental value.

Fragment ions

The formation of fragment ions has two main pathways. One is direct cleavage of C–C bond to generate both neutral and ionic radicals $C_nH_{2n+1}^+$ ($n = 4$–11); The other occurs via a β-H shift forming alkene ions $C_nH_{2n}^+$ ($n = 5$–10) and alkanes.

Figure 3 displays photoionization efficiency spectra of main radical ions $C_nH_{2n+1}^+$ ($n = 4$–11). The AEs of $C_4H_9^+$, $C_5H_{11}^+$, $C_6H_{13}^+$, $C_7H_{15}^+$, $C_8H_{17}^+$, $C_9H_{19}^+$, $C_{10}H_{21}^+$, and $C_{11}H_{23}^+$ are 10.78, 10.76, 10.72, 10.64, 10.56, 10.52, 10.48, and 10.45 eV, respectively, indicating a trend of decrease of AEs with the increase of *m*/*z*. The dissociation energies of octadecane were also calculated theoretically (Table 1). They are calculated to be 11.02 eV for $C_4H_9^+ + C_{14}H_{29}$, 10.84 eV for $C_5H_{11}^+ + C_{13}H_{27}$, 10.81 eV for $C_6H_{13}^+ + C_{12}H_{25}$, 10.80 eV for $C_7H_{15}^+ + C_{11}H_{23}$, 10.78 eV for $C_8H_{17}^+ + C_{10}H_{21}$, 10.77 eV for $C_9H_{19}^+ + C_9H_{19}$, 10.68 eV for $C_{10}H_{21}^+ + C_8H_{17}$, 10.66 eV for $C_{11}H_{23}^+ + C_7H_{15}$ with respect to neutral $C_{18}H_{38}$, which are a little larger than the experimental values. The bond order of octadecane ion was obtained on the basis of Wiberg bond index matrix in the NAO basis. It is calculated to be 1.0244, 0.8804, 0.0064, 0.005, 0.0047, 0.0043, 0.0034, 0.0029, and 0.0019 for C^1–C^2, C^2–C^3, C^3–C^4, C^4–C^5, C^5–C^6, C^6–C^7, C^7–C^8, C^8–C^9, and C^9–C^{10} (the number of C atom starts from one end of alkyl chain), respectively, indicating that the corresponding strength of C–C bond decreases continuously, which is agreeing with the results of AEs.

The main alkene ions include $C_5H_{10}^+$, $C_6H_{12}^+$, $C_7H_{14}^+$, $C_8H_{16}^+$, $C_9H_{18}^+$, and $C_{10}H_{20}^+$. The corresponding AEs are found to be 10.56, 10.52, 10.48, 10.45, 10.43, and 10.42 eV, respectively, obtained by the PIE spectra in Fig. 4. Different with direct dissociation into $C_nH_{2n+1}^+$ ions,

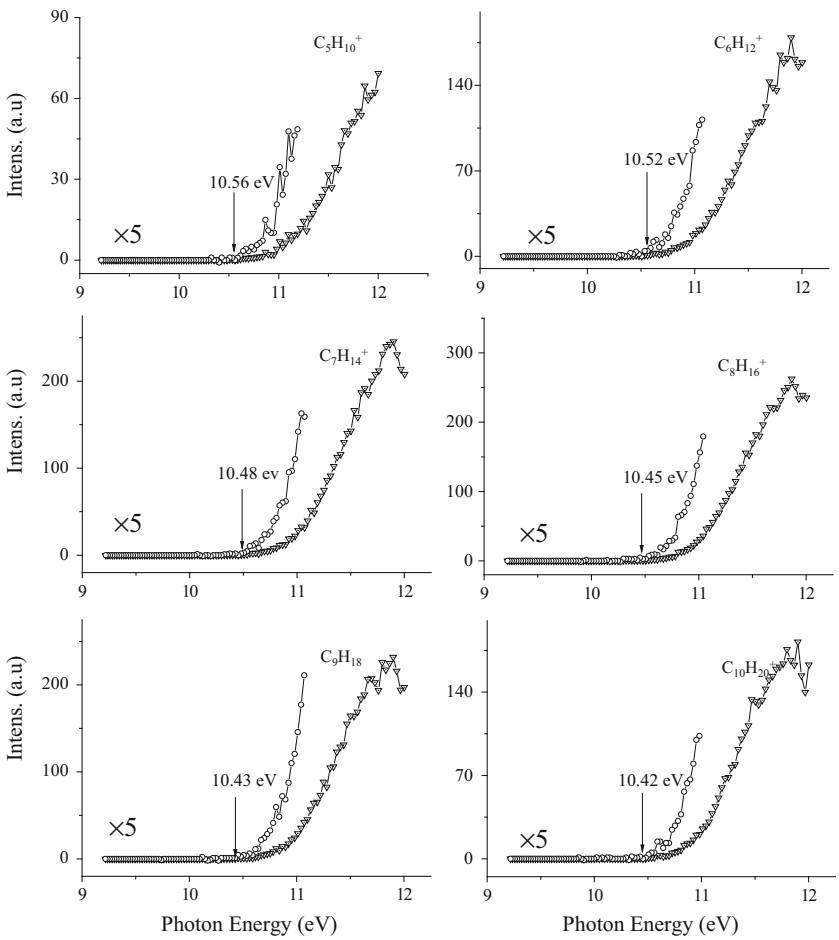

Fig. 4 PIE spectra of $C_nH_{2n}^+$ alkene ions

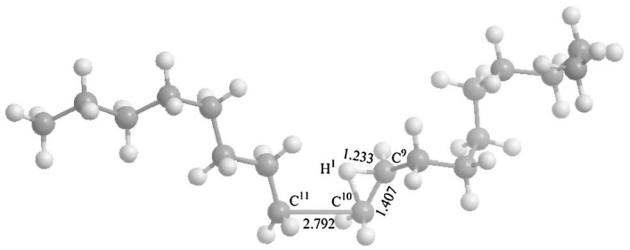

Fig. 5 Geometry and selected structural parameters (in Å) optimized at the B3LYP//6-31+G(d,p) level for TS6

alkene ions ($C_nH_{2n}^+$) are formed through a β-H shift transition state (TS). That is, octadecane needs to overcome transition state TS1, TS2, TS3, TS4, TS5, and TS6 to form $C_5H_{10}^+ + C_{13}H_{28}$ (calcd 10.28 eV), $C_6H_{12}^+ + C_{12}H_{26}$ (10.23 eV), $C_7H_{14}^+ + C_{11}H_{24}$ (10.20 eV), $C_8H_{16}^+ + C_{10}H_{22}$ (10.18 eV), $C_9H_{18}^+ + C_9H_{20}$ (10.17 eV), and $C_{10}H_{20}^+ + C_8H_{18}$ (10.17 eV), respectively. In this process, one C–C bond of octadecane is broken, and then with the help of the bend of C–C skeleton, a hydrogen atom from the β-carbon atom migrates to the other radical carbon, forming a neutral alkane and an alkene ion. For example, in transition state TS6 (Fig. 5), the C^{10}–C^{11} bond is calculated to be 2.792 Å, suggesting that it has been broken. The C^9–H^1 bond in TS6 is elongated from 1.096 Å in octadecane to 1.233 Å, while the C^9–C^{10} bond is shorten from 1.515 to 1.407 Å. With respect to neutral octadecane, the energy barrier is calculated to be 10.82 eV for TS1, 10.75 eV for TS2, 10.70 eV for TS3, 10.68 eV for TS4, 10.64 eV for TS5, 10.58 eV for TS6, suggesting that the β-H shift process is the rate-determining step for formation of alkene ions. Although the AEs of alkene ions are less than those of radical ions, formation alkene ions is less kinetically favorable, because it experiences a complex H shift process compared with a simple direct dissociation into radical ions. All these are according with the experimental results.

Conclusion

The photoionization and fragmentation of octadecane have been investigated with IRLD/VUV PIMS and theoretical calculations. The ionization energy of octadecane was measured to be 9.54 ± 0.05 eV and calculated to be 9.46 eV. The main fragment ions were assigned to radical ions ($C_nH_{2n+1}^+$, $n = 4$–11) and alkene ions ($C_nH_{2n}^+$, $n = 5$–10). The AEs of fragment ions were obtained by measuring the photoionization efficiency spectrum. The AE values of both $C_nH_{2n+1}^+$ and $C_nH_{2n}^+$ decrease with the increase of the number of C atom. The radical ions $C_nH_{2n+1}^+$ are formed through a direct cleavage of C–C bond in octadecane, while yielding alkene ions $C_nH_{2n}^+$ needs to experience a β-H shift process. This work could be considered as an approach of a combination of IRLD/VUV PIMS and theoretical calculations to research of petroleum.

Acknowledgments This work was supported by the Program for NSFC (21003158), Promotive Research Fund for Excellent Young and Middle-aged Scientists of Shandong Province (BS2012NJ015), and the Fundamental Research Funds for the Central Universities (12CX02014A and 14CX02004A).

References

1. Seki H, Kumata F (2000) Structural change of petroleum asphaltenes and resins by hydrodemetallization. Energy Fuels 14(5):980–985
2. Ancheyta J, Centeno G, Trejo F, Marroquín G, García JA, Tenorio E, Tomes A (2002) Extraction and characterization of asphaltenes from different crude oils and solvents. Energy Fuels 16(5):1121–1127
3. Cho Y, Na JG, Nho NS, Kim S, Kim S (2012) Application of saturates, aromatics, resins, and asphaltenes crude oil fractionation for detailed chemical characterization of heavy crude oils by Fourier transform ion cyclotron resonance mass spectrometry equipped with atmospheric pressure photoionization. Energy Fuels 26(5):2558–2565
4. Goncalves S, Castillo J, Fernández A, Hung J (2004) Absorbance and fluorescence spectroscopy on the aggregation behavior of asphaltene–toluene solutions. Fuel 83(13):1823–1828
5. Martínez-Haya B, Hortal AR, Hurtado P, Lobato MD, Pedrosa JM (2007) Laser desorption/ionization determination of molecular weight distributions of polyaromatic carbonaceous compounds and their aggregates. J Mass Spectrom 42(6):701–713
6. Chen X, Shen B, Sun J, Wang C, Shan H, Yang C, Li C (2012) Characterization and comparison of nitrogen compounds in hydrotreated and untreated shale oil by electrospray ionization (ESI) Fourier transform ion cyclotron resonance mass spectrometry (FT-ICR MS). Energy Fuels 26(3):1707–1714
7. Lob A, Buenafe R, Abbas NM (1998) Determination of oxygenates in gasoline by FTIR. Fuel 77(15):1861–1864
8. Lonnon DG, Hook HM (2003) ^{17}O quantitative nuclear magnetic resonance spectroscopy of gasoline and oxygenated additives. Anal Chem 75(17):4659–4666
9. Mühlberger F, Streibel T, Wieser J, Ulrich A, Zimmermann R (2005) Single photon ionization time-of-flight mass spectrometry with a pulsed electron beam pumped excimer VUV lamp for online gas analysis: setup and first results on cigarette smoke and human breath. Anal Chem 77(22):7408–7414
10. Cool TA, Nakajima K, Taatjes CA, McIlroy A, Westmoreland PR, Law ME, Morel A (2005) Studies of a fuel-rich propane flame with photoionization mass spectrometry. Proc Combust Inst 30(1):1681–1688
11. Mysak ER, Wilson KR, Jimenez-Cruz M, Ahmed M, Baer T (2005) Synchrotron radiation based aerosol time-of-flight mass

spectrometry for organic constituents. Anal Chem 77(18):5953–5960
12. Hansen N, Cool TA, Westmoreland PR, Kohse-Hoinghaus K (2009) Recent contributions of flame-sampling molecular-beam mass spectrometry to a fundamental understanding of combustion chemistry. Prog Energy Combust 35(2):168–191
13. Kameta K, Kouchi N, Ukai M, Hatano Y (2002) Photoabsorption, photoionization, and neutral-dissociation cross sections of simple hydrocarbons in the vacuum ultraviolet range. J Electron Spectrosc Relat Phenom 123(2–3):225–238
14. Person JC, Nicole PP (1968) Isotope effects in the photoionization yields and the absorption cross sections for ethylene and *n*-Butane. J Chem Phys 49:5421–5426
15. Schoen RI (1962) Absorption, ionization, and ion-fragmentation cross sections of hydrocarbon vapors under vacuum-ultraviolet radiation. J Chem Phys 37:2032–2040
16. Adam T, Zimmermann R (2007) Determination of single photon ionization cross sections for quantitative analysis of complex organic mixtures. Anal Bioanal Chem 389(6):1941–1951
17. Wang J, Yang B, Cool TA, Hansen N, Kasper T (2008) Near-threshold absolute photoionization cross-sections of some reaction intermediates in combustion. Int J Mass Spectrom 269(3):210–220
18. Zhou Z, Zhang L, Xie M, Wang Z, Chen D, Qi F (2010) Determination of absolute photoionization cross-sections of alkanes and cyclo-alkanes. Rapid Commun Mass Spectrom 24(9):1335–1342
19. Pan Y, Zhang L, Zhang T, Guo HJ, Hong X, Qi F (2008) Photoionization studies on various quinones by an infrared laser desorption/tunable VUV photoionization TOF mass spectrometry. J Mass Spectrom 43(12):1701–1710
20. Pan Y, Zhang TC, Hong X, Zhang YW, Sheng LS, Qi F (2008) Fragment-controllable mass spectrometric analysis of organic compounds with an infrared laser desorption/tunable vacuum ultraviolet photoionization technique. Rapid Commun Mass Spectrom 22(10):1619–1623
21. Frisch MJ, Trucks GW, Schlegel HB, Scuseria GE, Robb MA, Cheeseman JR, Scalmani G, Barone V, Mennucci B, Petersson GA, Nakatsuji H, Caricato M, Li X, Hratchian HP, Izmaylov AF, Bloino J, Zheng G, Sonnenberg JL, Hada M, Ehara M, Toyota K, Fukuda R, Hasegawa J, Ishida M, Nakajima T, Honda Y, Kitao O, Nakai H, Vreven T, Montgomery JJA, Peralta JE, Ogliaro F, Bearpark MJ, Heyd J, Brothers EN, Kudin KN, Staroverov VN, Kobayashi R, Normand J, Raghavachari K, Rendell AP, Burant JC, Iyengar SS, Tomasi J, Cossi M, Rega N, Millam NJ, Klene M, Knox JE, Cross JB, Bakken V, Adamo C, Jaramillo J, Gomperts R, Stratmann RE, Yazyev O, Austin AJ, Cammi R, Pomelli C, Ochterski JW, Martin RL, Morokuma K, Zakrzewski VG, Voth GA, Salvador P, Dannenberg JJ, Dapprich S, Daniels AD, Farkas Ö, Foresman JB, Ortiz JV, Cioslowski J, Fox DJ (2009) Gaussian 09. Gaussian Inc., Wallingford
22. Becke AD (1993) Density-functional thermochemistry. III. The role of exact exchange. J Chem Phys 98(7):5648–5652
23. Deng L, Zhang L, Guo H, Jia L, Pan Y, Hao Yin H, Qi F (2010) VUV photon-induced ionization/dissociation of antipyrine and propyphenazone: mass spectrometric and theoretical insights. J Mass Spectrom 45(7):734–739
24. Glendening ED, Reed AE, Carpenter JE, Weinhold F (1996) NBO version 3.1. Theoretical Chemistry Institute, University of Wisconsin, Madison, WI
25. Guo WY, Bi YC, Guo HJ, Pan Y, Qi F, Deng WA, Shan HH (2008) Infrared laser desorption/vacuum ultraviolet photoionization mass spectrometry of petroleum saturates: a new experimental approach for the analysis of heavy oils. Rapid Commun Mass Spectrom 22(24):4025–4028
26. Jochims HW, Schwell M, Chotin JL et al (2004) Photoion mass spectrometry of five amino acids in the 6-22 eV photon energy range. Chem Phys 298(1):279–297
27. Schwell M, Jochims HW, Baumgärtel H, Clemino M, Dulieu F, Baumgartel H, Leach S (2008) VUV photophysics and dissociative photoionization of pyrimidine, purine, imidazole and benzimidazole in the 7–18 eV photon energy range. Chem Phys 353(1):145–162
28. Linstrom PJ, Mallard WG (2005) NIST Chemistry webbook No. 69. National Institute of Standard and Technology, Gaithersburg, MD. http://webbook.nist.gov
29. Chupka WA (1971) Effect of thermal energy on ionization efficiency curves of fragment ions. J Chem Phys 54(5):1936–1947
30. Guyon PM, Berkowitz J (1971) Interpretation of photoionization threshold behavior. J Chem Phys 54(4):1814–1826
31. Steiner B, Giese CF, Inghram MG (1961) Photoionization of alkanes. Dissociation of excited molecular ions. J Chem Phys 34(1):189–220